International Journal of Heat and Mass Transfer 160 (2020) 120173

Contents lists available at ScienceDirect

International Journal of Heat and Mass Transfer

journal homepage: www.elsevier.com/locate/hmt

Heat transfer and structure of pulsating flow behind a rib

I.A. Davletshin*, A.N. Mikheev, N.I. Mikheev, R.R. Shakirov

Institute of Power Engineering and Advanced Technologies, FRC Kazan Scientific Center, Russian Academy of Sciences, 2/31 Lobachevskogo Str., Kazan 420111, Russia

ARTICLE INFO

Article history:
Received 1 May 2020
Revised 23 June 2020
Accepted 4 July 2020

Keywords:
Flow separation
Pulsating flow
Forcing frequency
Forcing amplitude
Heat transfer coefficient
Flow structure
Turbulent characteristics

ABSTRACT

The paper elaborates on experimental studies of heat transfer and kinematic structure of steady and pulsating air flows past a spanwise rib. The forcing frequency range of (0–30) Hz is considered, and the normalized forcing amplitude of velocity is 0.5. Forced flow pulsations are shown to enhance heat transfer if compared to the steady-state flow, particularly in the near-wake region behind the rib. Experimental data on the heat transfer coefficient in pulsating flows are best generalized using the non-dimensional pulsation frequency (Strouhal number). Profiles of velocity and turbulent parameters are demonstrated at a number of representative coordinates along the separation region. The dynamics of the kinematic structure of pulsating flows is described using the profiles of parameters in different phases of forced flow pulsations. The correlation between local heat transfer in the separation region and local hydrodynamic parameters is analyzed. The distribution of heat transfer coefficient over the wall in the rib wake correlates best with the distributions of transverse velocity component.

1. Introduction

Flow separation is a common phenomenon encountered in nature and engineering. Chang [1] described different types of separated flows in detail. In engineering, flow separation is considered unfavorable when it promotes hydraulic loss. At the same time, it can be beneficial for heat and mass transfer enhancement.

Flow separation in channels is attributed to complex geometry of these channels. The structure of separated flows features separation and reattachment points (lines) as well as a recirculation region. The flow pattern is further complicated by the pulsating behavior of flow parameters even under steady boundary conditions.

Flows past obstacles are a common type of separated channel flows. The shape and location of obstacles have a major impact on the kinematic structure and heat transfer [2]. In particular, such flows are observed in electronic devices, in which certain thermal condition must be maintained. In these cases, the shape and location of heat releasing roughness elements (ribs) can be essential for cooling [3]. In general, different shapes of obstacles (twisted spirals, V-shaped ribs, grooves, dimples, etc.) can be employed for enhancement of transfer processes in channels [4,5]. Such elements (both single and in arrays) can increase heat transfer manifold if compared to smooth channels. Channels with discrete roughness elements exhibit two- three-fold augmentation of heat transfer [6–14].

According to currently available research data, the distributions of heat transfer coefficient behind both backward-facing steps and ribs are non-monotonic with a minimum near the obstacle and a maximum close to the reattachment point. Heat transfer can be estimated using different empirical correlations, e.g. its maximum values can be drawn from generalization made in [15].

Forced flow pulsations induce standing or traveling waves in flows [16,17] entailing specific patterns of hydrodynamics and heat transfer in the channels, including the resonance. Such flows have two additional governing parameters: frequency and amplitude of pulsations [18–20]. However, it may also appear necessary to take into account the wave shape (velocity variation pattern) [20]. Meanwhile, the majority of research papers deal with a harmonic or close to harmonic pulsation pattern.

Hydrodynamics and heat transfer in separated flows subjected to forced pulsations of velocity (flow rate) are considerably more complicated [21–24]. Pulsations can be generated, among other methods, by acoustic impact on the flow [25]. Heat transfer in such flows grows with the increase in the Reynolds number and pulsation amplitude similarly to backward-facing step flows [26,27]. Forced flow pulsations can cause fundamental rearrangement of separated flows. Experiments in [22] revealed reduction in the reattachment length behind an orifice as well as heat transfer aug-

* Corresponding author.
E-mail address: davlet60@mail.ru (I.A. Davletshin).

https://doi.org/10.1016/j.ijheatmasstransfer.2020.120173
0017-9310/

Nomenclature

A_U	amplitude of velocity pulsations, m/s
f	frequency, Hz
e	rib height, m
H	channel height, m
h	heat transfer coefficient, W/(m^2•K)
Nu=he/λ	Nusselt number
Q	heat flux, W; or volumetric flow rate, m^3/s
$Re=U_0e/\nu$	Reynolds number
R	electrical resistance, Ω
St=fe/U_0	Strouhal number
T	temperature, °C (K)
U	streamwise velocity component, m/s; or voltage, V
U_0	bulk velocity at the channel inlet, m/s
V	transverse velocity component, m/s
x, y	coordinates, m
X_R	flow reattachment coordinate (reattachment length), m

Greek symbols

τ	time, s
$\beta= A_U/U_0$	normalized amplitude of flow velocity
φ	phase angle of velocity pulsations, deg
λ	thermal conductivity, W/(m•K)
$\omega=\partial V/\partial x-\partial U/\partial y$	flow vorticity, 1/s

Subscripts

i	number of track
w	wall
st	steady flow
p	periodic

mentation of up to 1.5 times in the separation region and up to 5 times in the immediate vicinity of the orifice (if compared to the steady flow case with the same average flow rate). Cukurel et al. [25] also documented the shifted location of maximum heat transfer coefficient in flows subjected to acoustic impacts of different frequencies and amplitudes in the vicinity of a square rib. However, they did not observe the same level of heat transfer enhancement as in [22]. Yet another technique to impact the flow structure is periodic blowing-suction through the edge of the rib. Such an approach was employed by numerous studies into backward-facing step flows [28–31]. These papers were mainly focused on the flow structure control. They documented the reattachment length reduction by an average of 30%. Rhee and Sung [32] studied heat transfer enhancement by periodic flow excitation through a slit on the backward-facing step edge [32]. They reported 40% increase in the heat transfer coefficient in the near wake of the step at the Strouhal number of 0.275.

From a practical perspective, the research results in this field can benefit different engineering developments: aircrafts, heat exchangers, pipeline systems, etc. They are also relevant for turbomachinery operating in steady and pulsating modes [33].

Intensive generation of regular vortices behind obstacles is a typical feature of pulsating separated flows [22,34]. These vortical structures are supposed to enhance the transfer processes. However, it should be noted that a reverse situation is also possible in this case. In high-frequency modes, stable vortices may exist near the wall impeding heat and mass transfer between the core flow and the near-wall region [34].

The present experimental research estimates the correlation between heat transfer in the separation region of the pulsating flow and its hydrodynamics.

2. Experimental setup and procedure

Heat transfer behind a rib in pulsating flows was studied using an experimental setup schematically shown in Fig. 1. The setup included a smoothly shaped inlet (position *1* in Fig. 1) and a test section (pos. *3*), which was a 0.115 × 0.15 m^2 rectangular channel with the length of 1.2 m. An aluminum square rib (pos. *6*) was installed on one of the 0.15 m wide walls at the distance of 100 mm from the inlet. The rib height was e = 30 mm (all three dimensions of the rib: 30 × 30 × 150 mm^3). Part of this same wall served as a 455 mm long measurement section (pos. *2*) for heat transfer experiments. Flow pulsations that followed close to harmonic pattern were generated at the channel outlet by a rotating flap (pos. *4*) fitted on the engine shaft. The axis of the flap was perpendicular to the channel axis. Pulsation frequency was set by adjustment of the engine shaft speed using Vacon 10 frequency converter. Besides, the amplitude of pulsations could be adjusted in the pulsator in the range of β=0–1. To this end, two windows were made in the pulsator. The first window was equipped with the rotating flap, while the second one was open. Adjusting the ratio between the open flow areas of these windows we set the required amplitude of forced flow pulsations. Detailed description of the pulsator is given in [35]. To maintain stable average flow rate, a 1.5 m^3 receiver tank was installed downstream of the pulsator. The air flow from the receiver was adjusted by opening an appropriate critical flow nozzle. The flow rate was generated by a compressor operating in a suction mode. Thus, the air with environmental parameters was supplied to the channel inlet. The air temperature was measured by a platinum resistance thermometer Pt100 (pos. *5*) installed in the smooth inlet (pos. *1*).

Heat transfer between the wall and the flow was provided by heating the measurement section by direct current supplied from a battery with the voltage E = 24 V. To that end, a printed circuit board with copper tracks was used as a channel wall. Simultaneously, these tracks served as resistance thermometers that measured local wall temperatures. Thus, the distribution of heat transfer coefficients was estimated from heat release values and temperature difference between the wall and the flow.

Normalized rib height (blockage ratio) in the channel was e/H = 0.26, where H = 115 mm is the channel height (Fig. 1). It should be noted that the canonical problem in this field is an unbounded flow past an obstacle: $e<<H$ ($e/H<<1$). In practice, it means that very small objects or channels with very large cross sections must be considered. In the former case, detailed (spatially resolved) studies of hydrodynamics and heat transfer in the separation region are challenging. In the latter case, experimental studies are quite expensive. Thus, the channel geometry studied in the present experiments is a compromise between these contradictive requirements. It allowed us to obtain detailed distributions of parameters in separated flows using reasonable dimensions of the experimental setup and reasonable flow rates.

The obtained data were analyzed under the assumption that the separated flow is two-dimensional. This assumption is valid for turbulent flows if the ratio between the channel width and the rib height is more than 10 [36]. However, many experimental studies considered significantly lower ratios (e.g. the ratio is 5 in [37]). Obviously, three-dimensionality of flows is progressively more pronounced with the decrease in the normalized channel width. But many authors treat such flows as two-dimensional in the axial plane, at least in terms of the averaged parameters.

In our case, this ratio was 150 mm/30 mm=5. So, in the framework of the above mentioned compromise and in application to the axial plane of the channel, we considered the flow to be two-dimensional. The influence of corners of the plane channel on hydrodynamics and heat transfer was neglected in this paper. Accord-

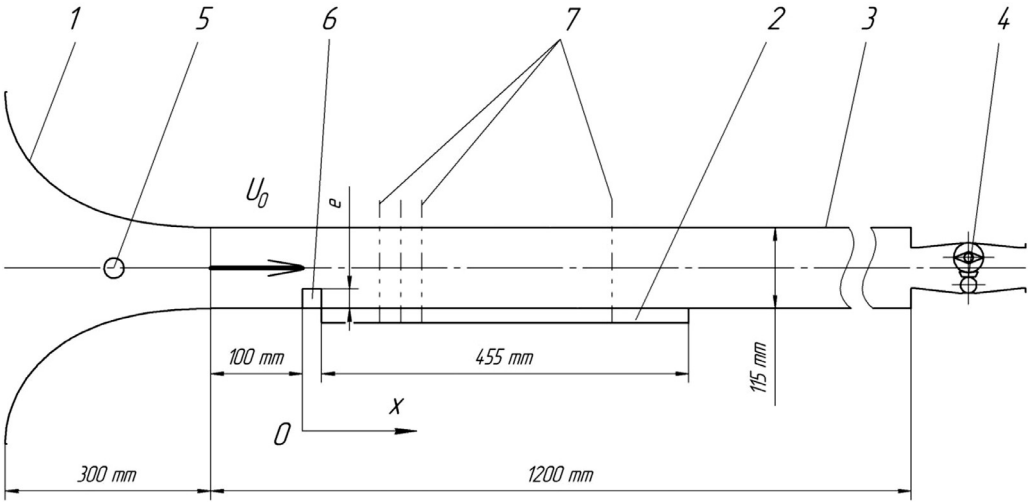

Fig. 1. Experimental setup: *1* – inlet; *2* – heated wall; *3* – channel; *4* – pulsator; *5* – thermometer; *6* – rib; 7 – sections in which flow parameters were measured.

ingly, the obtained results are valid for the axial (central) plane of the channel under consideration.

3. Measurement techniques

The employed method consists in heating of the surface with simultaneous estimation of its local temperature on the basis of the measured electrical resistance of the heating element associated with this temperature. To that end, the heated wall (pos. *2* in Fig. 1) spanning across the whole channel width was embedded into some part of the test section wall (Fig. 1). This heated wall was a printed circuit board (PCB) with the length of 455 mm and the thickness of 1.5 mm. Zigzag tracks were etched on the copper plating of PCB that faced toward the channel interior. There were a total of 47 copper tracks localized in rectangular regions with the areas of 150 × 9.5 mm^2. Each region had its own contacts that could be connected to the current source in series or parallel circuit. Central segments of tracks with the size of 80 × 9.5 mm^2 had electrical contacts for voltage drop measurement. These contacts (copper tracks on the reverse side of PCB) were connected to terminals and further to an analog-to-digital converter and PC. Voltage drop across each heating element was measured in order to estimate the heat generation and electrical resistance of segments of tracks and hence the temperatures of wall regions using the temperature-resistance relation. Prior to these measurements, calibration curves of electrical resistance of tracks, R_i, vs temperature were plotted. For illustrative purposes, Fig. 2 shows only a few calibration curves, and the rest of them are similar in both the behavior and values. A constant climate cabinet was employed for these measurements. The temperature was controlled by a platinum thermometer Pt100 with the accuracy of 0.3°C. During the resistance measurements, the electric current supplied to the tracks was the same as during the PCB heating in the mode of heat flux measurement, but the pulse duration was short (no more than 0.2 s). This pulse duration allowed neglecting the variation of track temperature during the calibration. The calibration data provided the resistance, R_{i0} of each track at the temperature T_0=0°C. Simultaneously, the temperature coefficient of resistance, α_t, included in $R_i=R_{i0}(1+\alpha_t(T_i-T_0))$ was estimated. This coefficient at T_0=0°C was close to the reference value for copper. The calibration yielded α_t=0.00421°C^{-1}, and the root-mean-square deviation of this value for all the tracks combined was $\sigma_{\alpha t}$=0.00004°C^{-1}. The experimental data were processed using individual R_{i0} for each track and one constant α_t=0.00421°C^{-1} for all tracks.

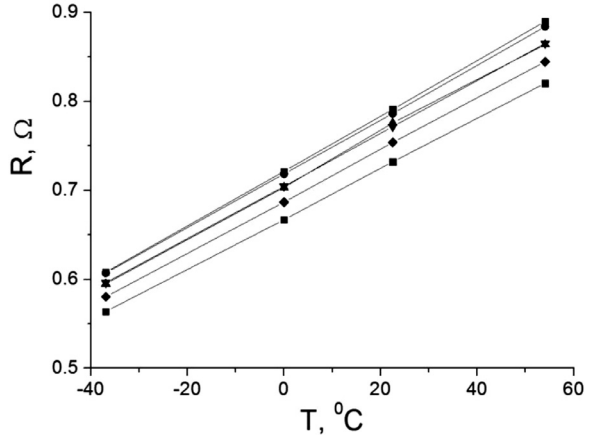

Fig. 2. Electrical resistance of tracks vs temperature.

The whole surface of the wall was heated by electrical current according to the boundary condition of the second kind, q=const. Temperature measurements were carried out in the central part of the wall where the temperature field is assumed to be uniform in spanwise direction. Under these conditions, the measuring section of PCB was essentially a set of resistance thermometers spaced 9.5 mm apart along the channel. The measurements yielded the values of heat flux and temperature on the heated wall.

The external surface of the heated wall was thermally insulated.

Local heat transfer coefficients corresponding to streamwise coordinates x_i were determined from the heat balance equation:

$$h_i = \frac{U_i I_i - Q_i^*}{F(T_i - T_f)},$$

where T_i is the local temperature of the wall; T_f is the flow temperature; U_iI_i is the heat generated by electrical current in the measurement section; Q_i^* is the heat losses; F is the section area. Q_i^* includes the heat loss through thermal insulation, radiation, thermal conductivity to the adjacent walls and heat fluxes between the adjacent tracks. The flow temperature, T_f, is the temperature measured at the channel inlet. Heating of the flow from the wall was neglected, because the maximum increase of the flow temperature at the end of the heated wall did not exceed 0.6 °C even at the minimal air velocity. The temperature growth was even less pronounced at higher velocities and close to the rib. This did not result in a noticeable increase of the uncertainty in heat transfer co-

efficient, because in all the considered flow regimes the air was heated by no more than 1.2% of the average temperature head, which ranged between 20 and 50°C. The description of measurement technique with the uncertainty analysis is provided in [34]. The uncertainty in measured temperature was shown to be the major source of uncertainty in the measurement result, h_i. The relative uncertainty reduces with the increase in the temperature head and does not exceed $\frac{\Delta Nu_i}{Nu_i} \sim 0.05$ at the temperature head of 20°C. At the temperature heads considered, the relative uncertainty in local heat transfer coefficient did not exceed 0.05.

The kinematic structure of flow was studied at several representative coordinates in the axial plane along the channel behind the rib. Channel walls were made of transparent materials (glass and polycarbonate). To visualize the flow structure, aerosol particles were supplied to the channel inlet from the conditioning chamber (air with MT-Gravity liquid particles with the medium density and the average particle size of about 0.1..5 μm; Safex aerosol generator). The light sheet was generated by a continuous diode-pumped laser (DPSS-Laser) KLM-532/5000-h. The flow patterns were recorded by a high-speed monochrome camera Fastec HiSpec with the frame resolution of 700 × 80 pix (scaling factor of 0.031 mm/pix), frame rate $f = 9259$ 1/s, video duration 3.5 s. The camera was equipped with a high-aperture lens Navitar 1″F/0.95 with a focal distance of 25 mm and manual focus control. Optical method SIV (Smoke Image Velocimetry) based on digital processing of recorded flow patterns was employed for measurements of the fields of velocity and Reynolds stresses. Velocity vector fields in this method are estimated from the displacements of turbulent structures visualized by the aerosol. Minimal size of the interrogation window used in this study was 16 × 6 pix (the short size positioned normal to the wall). These measurements enabled to analyze the kinematic structure of turbulent separated flows. Detailed description of the measurement technique as well as its application are given in [38–40]. The uncertainty of SIV measurements was analyzed by Molochnikov et al. [39]. They showed that the main source of uncertainty in measured components of velocity vectors is a random error in estimation of frame-to-frame displacement of the image, and the total absolute uncertainty in SIV measurements does not exceed 0.039 pix. For the spatial resolution and the frame rate chosen for the current research, the root-mean-square deviation of velocity components is 0.03 m/s.

SIV measurements yielded the profiles of streamwise and transverse components of velocity, fluctuations of streamwise and transverse velocities, Reynolds stress and vorticity, ω, at the representative coordinates of the separated flow.

4. Results of heat transfer studies

Heat transfer was studied for the following ranges of parameters. Bulk velocity in the channel $U_0=Q/F_0=$(1.7 – 6.35) m/s (Q – volumetric flow rate, F_0 – cross section area of the channel). It should be noted that the receiver tank included in the experimental setup guaranteed stable constant time-averaged flow rate through the channel. Flow pulsations (about the average flow rate Q) were limited to the test section exclusively. The Reynolds number based on the rib height was $Re=U_0e/\nu=$(3400 – 12,700), which provided turbulent flow in the separation region. The flows with minimal velocities (Re=3400) corresponded to the boundaries of the turbulent flow range [41]. Forced velocity pulsations were generated in the frequency range of f=(0 – 30) Hz with a normalized amplitude $\beta=A_U/U_0$~0.5.

Fig. 3 demonstrates the measured distributions of heat transfer coefficient. The upstream edge of the rib is taken as x=0 coordinate. For illustrative purposes, the rib is shown as a black square in the figure with a proper scale and location relative to x-coordinate. The heat transfer coefficient is plotted in a non-dimensional form

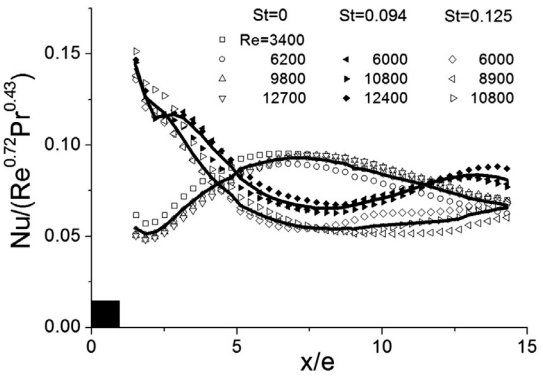

Fig. 3. Heat transfer coefficient in the separation region behind the rib.

as $Nu/(Re^{0.72}Pr^{0.43})$. The Nusselt number is based on the rib height, $Nu=he/\lambda$. The correlation $Nu=0.0803Re^{0.72}Pr^{0.43}$ taken for reference was suggested in [15] as an approximation of a large amount of experimental results on heat transfer in the separation region near the reattachment point reported by different authors. However, authors [15] employed the length of the dividing streamline (~reattachment length) as a linear scale. It appeared that when we used $Re^{0.72}$ for data generalization, the distributions of heat transfer coefficient over the whole length of the separation region were independent of the Reynolds number both in steady and pulsating flows. The effect of forced flow pulsations is best generalized using the non-dimensional pulsation frequency (Strouhal number), $St=fe/U_0$. It has to be noted here that the normalized amplitude of flow pulsations remained at the same level in all experiments. Curves in Fig. 3 show that the distributions of heat transfer coefficient coincide at certain St numbers (with a scatter lying within the range of reproducibility of experimental results). The lines in the figure are the averaged distributions for St=0, 0.094 and 0.125, while the dots are experimental data. Each considered mode had its own individual Strouhal number because of the incremental adjustment of frequency (by frequency converter) and flow rate (by a set of critical flow nozzles). Accordingly, during the analysis, the results that were grouped together were actually obtained at slightly different Strouhal numbers. In pulsating flows, the Strouhal number stayed within the intervals of St=0.094±0.010 and St=0.125±0.010, while in the steady flow it was unambiguously equal to 0.

Experiments showed that heat transfer averaged over the length of the separation region was enhanced in pulsating flows compared to the steady-state flows due to significant heat transfer augmentation in the near wake of the rib. The increase in the forcing frequency makes the peak heat transfer shift toward the rib. Almost three-fold enhancement of heat transfer is observed in the immediate vicinity of the rib if compared to the same wall coordinate in steady flows. Further downstream, the heat transfer level in pulsating flows becomes lower than that in steady flows and then approaches the steady flow values. It is noteworthy that similar effect was observed in [22]. However, the Strouhal number in [22] was based on the reattachment length (the coordinate of peak heat transfer) and the following physical interpretation was provided: when St=1, the distance traveled by the flow during one period of forced pulsations is equal to the reattachment length.

5. Kinematic structure of flow

The flow patterns were studied in detail at the bulk velocity U_0=1.7 m/s (Re=3400). For pulsating flows, first of all, the frequency of forced velocity pulsations was checked using the oscillograms, and the pulsation amplitude was estimated. Fig. 4 demon-

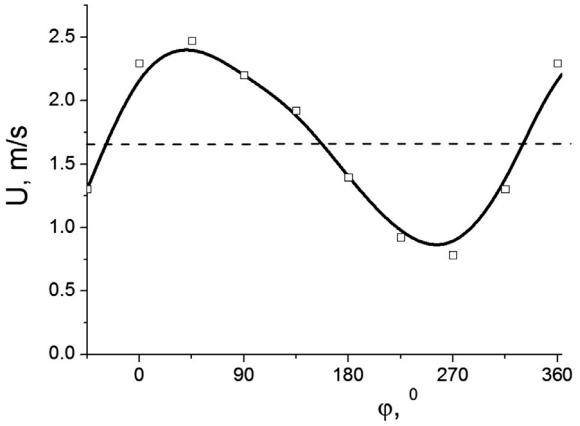

Fig. 4. Pattern of velocity variation.

strates velocity behavior in the core flow ($y/e = 2.4$) at $x/e = 3$. This curve is essentially an averaged oscillogram of velocity. Each point of the curve was derived by averaging over a large number of periods of forced pulsations at the phase angle $\Delta\varphi$=45°, where φ=$2\pi f\tau$. The phase angle was zero, φ=0, when the reference velocity reached the average level in the acceleration phase. Velocity oscillogram at a given point of undisturbed flow (outside the separation region) was used as a reference signal. As Fig. 4 shows, the normalized amplitude of forced velocity pulsations, β=(U_{max} – U_{min})/(U_{max} + U_{min}), is 0.52. Notice that the normalized amplitude of pulsations in the oncoming flow is employed for description of flow patterns. When the obstacle height is relatively small compared to the channel height, the amplitude of pulsations in the core flow is close to this value. However, at other points, especially in the separation region and close to it, the local values of β are different and can reach β>1 if reverse flows occur.

The kinematic structure of flow was studied successively at certain coordinates by measurement of velocity fields in narrow transverse stripes of the channel central plane instead of the whole flow at once. The measurement area was reduced in order to provide high space-time resolution of the profiles of velocity and turbulent parameters. These profiles were obtained in steady and pulsating flows (f = 10 Hz, St=0.176).

Positions of the time-averaged profiles in Fig. 5 indicate their x-coordinates. Measurements were performed in the flow region that was most affected by forced flow pulsations, x/e = 1.05 – 10. At the first coordinate (x/e = 1.05), the measurements were carried out immediately behind the rib, at the normalized distance of 0.05 from its downstream edge. All parameters are normalized by the bulk velocity, U_0. Dashed lines refer to the steady flow, while solid lines refer to the pulsating flow with the frequency f = 10 Hz (St=0.176). The coordinates are normalized by the rib height, e. For illustrative purposes, the horizontal dashed line in the figure marks the rib top.

The obtained measurements were analyzed with the assumption of two-dimensional flow at least in the axial plane in which measurements were performed. Each velocity component in steady turbulent flow was considered as a sum of averaged (overlined) and turbulent velocities:

$$U = \bar{U} + U', V = \bar{V} + V'.$$

The periodic velocity (denoted with a tilde mark) was added when pulsating turbulent flows were considered:

$$U = \bar{U} + \tilde{U} + U', V = \bar{V} + \tilde{V} + V',$$
where $\tilde{U} = A_U \mathrm{Sin}(2\pi f\tau)$.

In Fig. 5, RMS turbulent fluctuations U' and V' are shown as pulsating components in steady flows, while the pulsating components in pulsating flows are the sums of RMS periodic and turbulent fluctuations:

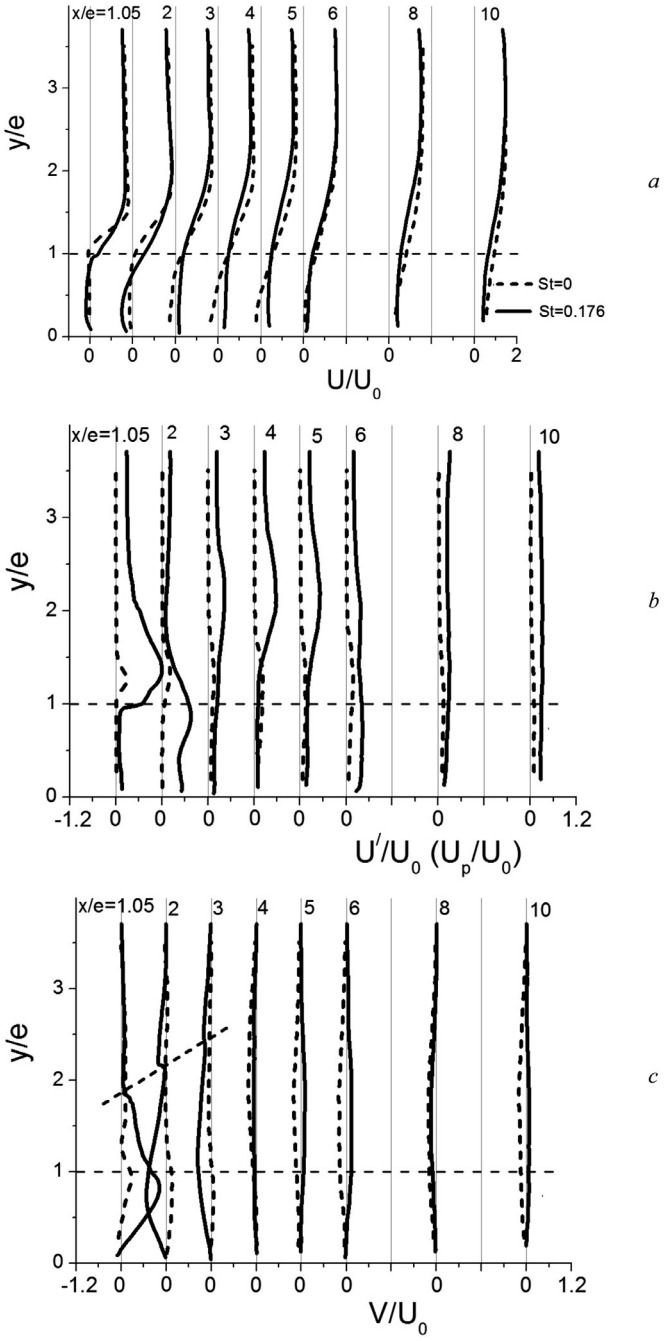

Fig. 5. Profiles of flow parameters in the separation region.

$$U_p = \tilde{U} + U', V_p = \tilde{V} + V'.$$

This is motivated by the fact that it is the combined effect of periodic forced pulsations and turbulent fluctuations that impacts the heat and mass transfer and momentum transport in the flows under consideration.

Overall, the hydrodynamic parameters measured in the steady flow agree well with the available data on separated flows. Profiles of streamwise velocity, U, exhibit the characteristic regions: core flow, reverse flow behind the rib, high transverse gradient in the mixing layer. Profiles of U yield the coordinate of the reattachment point, X_R, at which $\partial U/\partial y\,|_w = 0$ condition is fulfilled on the wall. $X_R \approx 6e$ in steady flows (Fig. 5, *a*). The reattachment point in pul-

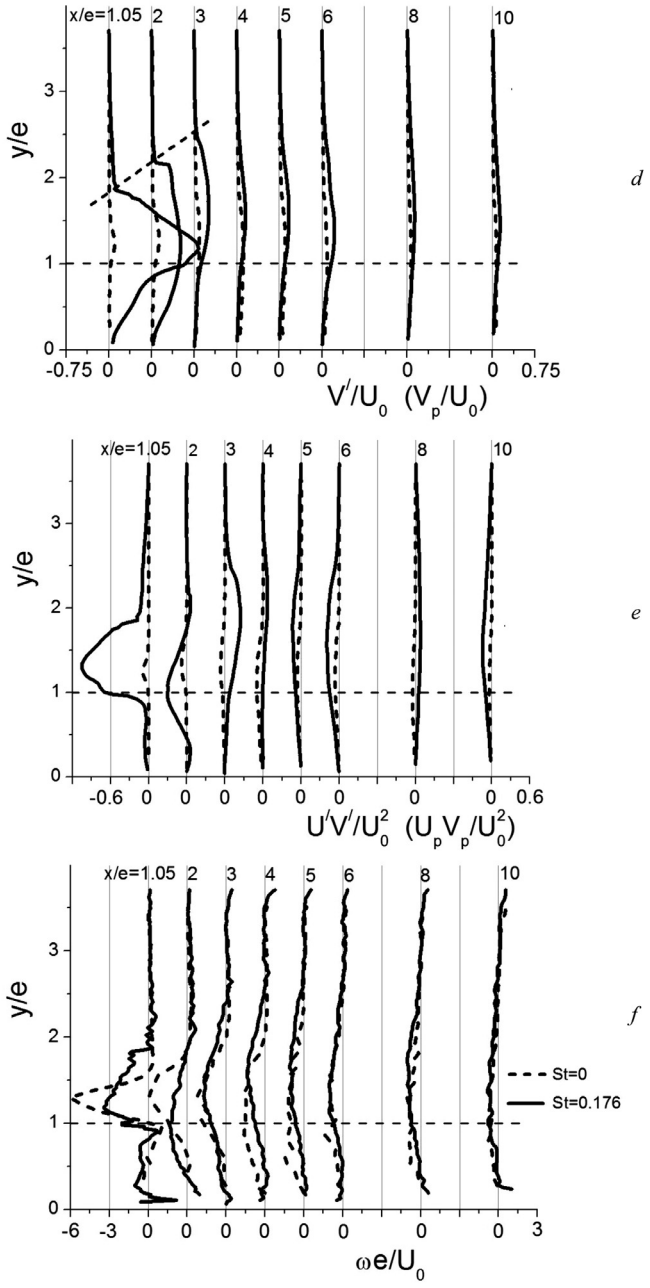

Fig. 5. Continued

be considered as additional verification of the employed measurement method.

The streamwise velocity profiles in pulsating flows, being almost equal to the steady flow case, exhibited smoother transition between the separation region and the core flow (Fig. 5, *a*), i.e. thicker (on average) shear layer. Forced flow pulsations make the pulsating components, U_p and V_p, increase manifold behind the rib (compared to U' and V'). Locations of these peak values in steady and pulsating flows are different. Generally, the peak values of U_p (Fig. 5, *b*) are located farther from the wall if compared to the peak values of U' in steady flows. Profiles of V (Fig. 5, *c*) and V_p (Fig. 5, *d*) exhibit some essential features. They have the points of sharp, almost abrupt, variation above the separation region. V and V_p are close to zero immediately behind the rib (at $x/e = 1.05$) in the undisturbed flow region ($y/e>1.9$). They grow fast near the rib (y/e~1.9) reaching local peaks at y/e~1. V and V_p also change abruptly at the point with the coordinates $x/e = 2$ and y/e~2.2. Here, the direction of transverse velocity, V, is opposite to the one at the previous coordinate, which suggests the vortical motion between the coordinates. V changes abruptly turning almost to zero. V_p profile exhibits the same abrupt variation at this coordinate. Similar behavior is observed further downstream at $x/e = 3$, y/e~2.5. However, the profile of transverse velocity, V, does not change abruptly here but only has an inflection point. Similarly, V_p profile exhibits smoother transition from almost zero (in the core) to high values closer to the separation region. Thus, the line connecting these specific points can be considered as a boundary between two regions of flow. It is shown by a dashed line in the figures. The flow is mostly undisturbed and vortex-free above this line. Below the line, the flow is disturbed by the rib, and large-scale vortices form, move and break down behind the rib in pulsating flows. The same is observed in the profiles of Reynolds stresses (Fig. 5, *e*) and vorticity (Fig. 5, *f*) – the above mentioned boundary line separates the region where these parameters are almost zero from the region with high Reynolds stresses and vorticity. The same well-defined boundary between the regions with and without vortices was documented in pulsating flow separating from a sharp inlet edge of the channel [34]. Note that the so-called vortex-free part of flow is not strictly free of vortices. The vortices, local in space or time, can still exist there. However, their strength, particularly its time-averaged value, is far less than in the disturbed region.

Indeed, flow visualization (Fig. 6) reveals a regular vortex street behind the rib (black square in the image) in pulsating flow. High level of velocity fluctuations in this region is associated with the dynamics of vortices. The analysis of hydrodynamics (Fig. 5) demonstrates that the vortices are localized mainly within $0<y/e<2.5$ for the considered channel geometry and flow modes.

sating flows is much closer to the rib: $X_R \approx 3e$. This fact complies with the reduced reattachment length in pulsating flows observed earlier [22].

Turbulent fluctuations of streamwise velocity component in steady flows agree well with [42] and exhibit approximately similar peak values U'/U_0~0.2 in the mixing layer, which are located above the separation region (Fig. 5, *b*). The coordinates of these peaks are somewhat different from [42]: y/e~1.3 instead of $y/e = 2.0 - 2.5$ [40]. This discrepancy can be attributed to the fact that Fouladi et al. [42] studied an unbounded rib flow in a wind tunnel, while the present paper deals with the separated flow in the channel of finite height ($y/e \le H/e = 3.83$). Turbulent fluctuations of transverse velocity component, V', behave similarly (Fig. 5, *d*). Their peak values are approximately equal to V'/U_0~0.1–0.15, which complies with the literature data on separated flows. It is noteworthy that comparison of results obtained in steady flows can

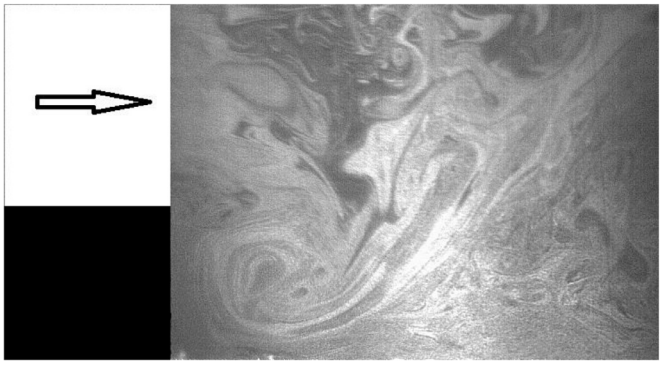

Fig. 6. Vortex formed behind the rib in pulsating flow at $f = 10$ Hz.

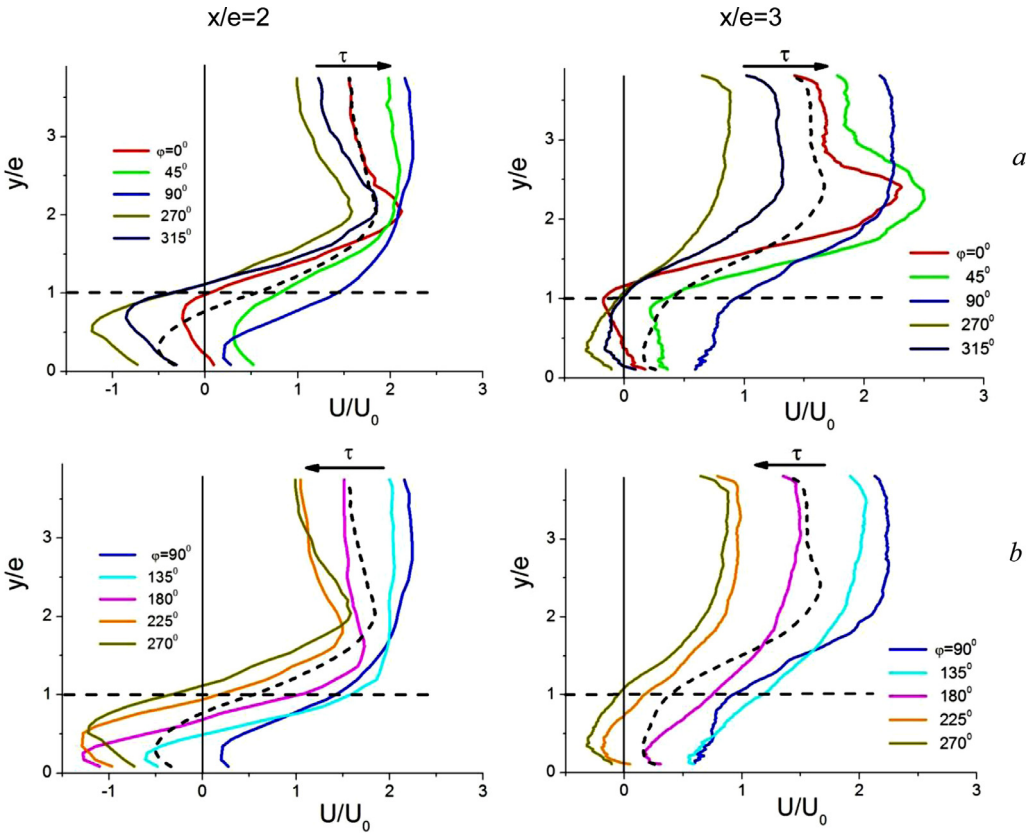

Fig. 7. Profiles of streamwise velocities at $x/e = 2$ (left column) and $x/e = 3$ (right column) in acceleration (a) and deceleration (b) phases.

Fluctuations are less pronounced in downstream regions, which can be attributed to disintegration of vortices.

The flow pattern shows that the vortex formed behind the rib approaches closest to the wall at the distance of ~e from the trailing edge of the rib (x/e~2). Obviously, vortices that regularly approach the wall induce strong fluctuations of flow parameters at this location, which is evident in U_p profile (Fig. 5, b) at $x/e = 2$. Here, the vorticity is also higher than the one at the nearest downstream coordinates (Fig. 5, f). High vorticity values at $x/e = 1.05$ at the altitude y/e~0.2 obviously indicate the existence of a corner vortex near the wall behind the rib.

Further information on the dynamics of processes in pulsating flows can be derived from the distributions of parameters over the phases of forced pulsations. Evolution of velocity profiles over a period of forced pulsations illustrates the flow patterns very efficiently. Fig. 7 shows the profiles of streamwise velocities at two representative coordinates, $x/e = 2$ and $x/e = 3$, corresponding to the recirculation zone and reattachment region, respectively. The profiles are plotted for two half-periods of forced pulsations (acceleration and deceleration of the main flow). Here, similarly to averaging of oscillograms, each velocity profile is obtained by averaging over a large number of pulsation periods in the range of the phase angles $\Delta\varphi$=45°. E.g. the profile for φ=0° was obtained by averaging in the range of ±22.5° around the average value φ=0°. Velocity profiles averaged over all phases (over the whole pulsation period) are included in Fig. 7 for comparison and shown by dash lines (solid lines in Fig. 5). It appeared that there are two groups of velocity profiles depending on their behavior: acceleration phase (Fig. 7, a) and deceleration phase (Fig. 7, b). In the acceleration phase, maximum acceleration is observed in the core flow, and the profiles are elongated in their central portion. At the moment of maximum acceleration (φ=0°), the flow decelerates at the height y~e. This fact indicates that a vortical structure with increasing rotation speed exists at this coordinate: the upper part of the vortex promotes flow acceleration in the channel center, while its lower part near to the rib decelerates the flow and even triggers reverse acceleration at $x/e = 3$. This is the pattern of pulsating flow (with vortices behind the rib) that was reported earlier in [22].

Velocity patterns in the flow deceleration phase exhibit somewhat different behavior. They are more uniform and filled, especially at $x/e = 3$. Their shapes at all phase angles are approximately the same. At minimal velocities, similarly to the preceding half-period, there is a reverse flow region near the wall, which is typical of separated flows. As expected, this is evident in the profiles plotted for $x/e = 2$. The velocity profiles retain this shape (with a local extremum near the wall) at somewhat higher velocities even when there is no reverse flow.

Such a difference in the patterns of velocity profiles is attributed to the dynamics of the vortex street formation. A vortex emerges and grows behind the rib in the flow acceleration phase. As soon as the velocity reaches its maximum, the vortex detaches from the rib and is swept to the flow, and then it breaks up due to viscous stresses. Accordingly, velocity profiles in this phase are subjected to a combined effect of two main components of motion: streamwise pulsations of the flow in general and vortical motion. It is the acceleration of vortical motion that “stretches” velocity profiles in the core flow when the velocity grows and “shrinks” them (inducing a brief period of reverse acceleration) at y/e~1 (Fig. 7, a). When the velocity decreases (Fig. 7, b), new vortex does not form and the vortex formed in the preceding half-period disintegrates. In this case, the velocity profiles retain their shape and follow the dynamics of forced velocity pulsations in this phase in an almost equidistant manner.

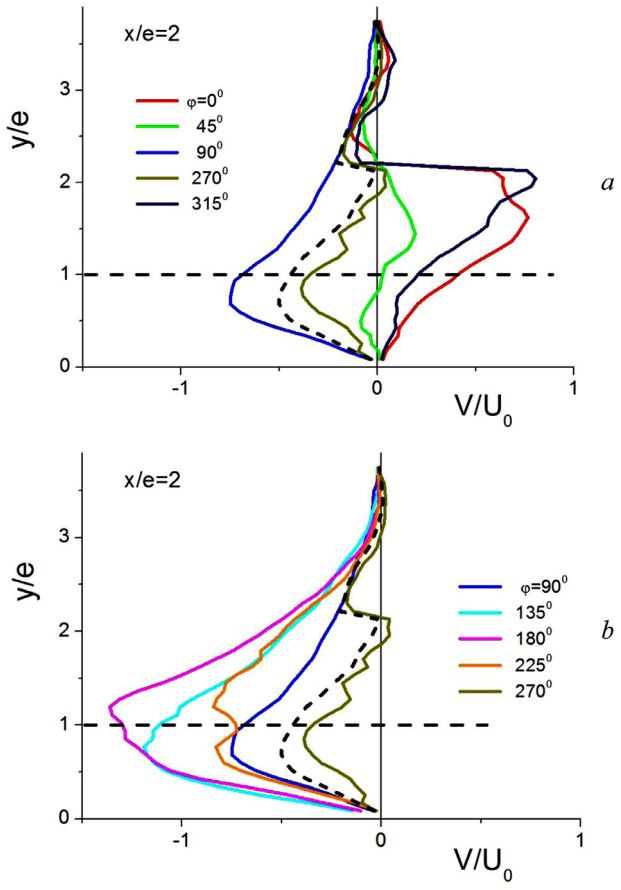

Fig. 8. Profiles of transverse velocities at $x/e = 2$ in acceleration (a) and deceleration (b) phases.

We mentioned above that the averaged profiles of transverse velocity, V, and its fluctuations (Fig. 5, c, d) have specific points most pronounced at $x/e = 2$. Profiles of V in different pulsation phases provide the insight into the mechanism that forms the kinematic structure of pulsating separated flows. Fig. 8 also shows these profiles in two different half-periods. Abrupt change in the transverse velocity is observed at y/e~2.2 in the phases of maximum flow acceleration (Fig. 8, a). It turns into zero and has extrema of opposite signs slightly above and below the y-coordinate of zero velocity. Such a profile of transverse velocity component can be attributed to a horizontal jet emerging in this region, which entrains the adjacent layers from above and below. The rate of fluid entrainment from above layers is almost constant throughout the period. Entrainment from below exhibits pronounced peaks at the moments of maximum flow acceleration. These moments are probably associated with vortices passing through this point. Jet localization coincides with the boundary separating the regions of high and almost zero vorticity suggested above.

In the flow deceleration phase, the gas from the core flow is supplied to the separation region (negative V, Fig. 8, b), filling the zone abandoned by the vortex after it had been shed to the flow.

The submitted idea is also clearly illustrated by the dynamics of the flow vorticity profile at the same coordinates, $x/e = 2$ and 3 (Fig. 9). The dashed line in the figure represents the vorticity profiles averaged over the whole period of forced pulsations. Similar grouping of vorticity profiles depending on the phases of velocity increase (Fig. 9, a) and decrease (Fig. 9, b) is also indicative of fundamental difference between these half-periods. Vorticity changes significantly in the phase of growing velocity. In other words, an active process of vortex generation is observed in this half-period. The figures show that vortices rotating in opposite directions can emerge at different heights in the channel. This is probably associated with the fact that these vortices belong to different regions (earlier referred to as vortex-free region and disturbed region). Thus, the presented data comply with the following flow pattern. Vortices with opposite rotation are formed on opposite sides of the boundary separating the described regions; local velocities of these vortices on the boundary match the main flow direction.

In the deceleration phase, the rate of vorticity variation is slower and no counter-rotating flows are observed at $x/e = 3$. In this case, flow vorticity values apparently characterize the separated recirculation flow behind the rib. During this half-period, regular vortical structures are not formed behind the rib edge as mentioned above.

The vorticity is high in the near-wall region of $x/e = 2$ section, which complies with the similar behavior of U_p fluctuations near the wall.

6. Correlation between heat transfer and flow parameters

For direct comparison with hydrodynamics, Fig. 10 demonstrates the heat transfer coefficient in steady and pulsating ($f = 10$ Hz) flows separately. Note that the position of reattachment points almost matches the points of maximum heat transfer. In steady flows, the heat transfer peaks at $x/e = 6.4$, while $X_R/e = 6$, as shown above. In pulsating flows, the heat transfer grows sharply as the distance from the rib is reduced and peaks in the immediate vicinity of the rib. However, the steep part of the curve exhibits a local "augmentation" of heat transfer. Such behavior (sometimes even featuring a local maximum) is typical of pulsating flows at St~0.094 (Fig. 3). This "augmentation" can probably be interpreted as relating to the reattachment region. In this case, this "peak" is located at $x/e = 2.5$ coordinate, so it is close to the coordinate of flow reattachment point, $X_R/e = 3$.

The combined analysis of hydrodynamics (Fig. 5) and heat transfer (Fig. 10) in pulsating flows reveals some correlation between them. Higher heat transfer coefficients correspond to higher level of fluctuations. Moving closer to the rib, we observe progressively stronger fluctuations of streamwise and transverse velocity, Reynolds stress, as well as heat transfer coefficient. However, the correlation is not as pronounced in steady flows. Nevertheless, it turned out that the correlation between heat transfer and hydrodynamics is expressed in the most explicit way when the normalized modulus of the transverse velocity component, $|V|/U_0$, is employed (Fig. 11). Maximum values of $|V|$ are taken from each profile to plot the curve in Fig. 10. Comparison between $|V|$ and

Nu (Fig. 10) demonstrates that they agree with each other at least qualitatively. It is reasonable to employ the modulus of transverse velocity for comparison, because, in fact, velocity of any direction provides mass transfer between the near-wall region and the core flow, and hence, promotes heat transfer between the wall and the flow.

Having confirmed the qualitative agreement, we searched for some quantitative correlation between the specified parameters of hydrodynamics and heat transfer. This correlation can be represented by Nu~($|V|/U_0$), which is plotted in Fig. 12. Each point in Fig. 12 corresponds to some local value of $\mathrm{Nu}/(\mathrm{Re}^{0.72}\mathrm{Pr}^{0.43})$ and a maximum modulus of the normalized transverse velocity $|V|/U_0$. These values are taken in pairs for specific x/e coordinates. Maximum values of the transverse velocity for each coordinate are derived from the profiles demonstrated in Fig. 5. Fig. 12 demonstrates the empirical data acquired at different coordinates, x/e, and different forcing frequencies, St. The line in the figure shows the power function

$$\mathrm{Nu}/\left(\mathrm{Re}^{0.72}Pr^{0.43}\right) = 0.13(|V|/U_0)^{0.26}. \quad (1)$$

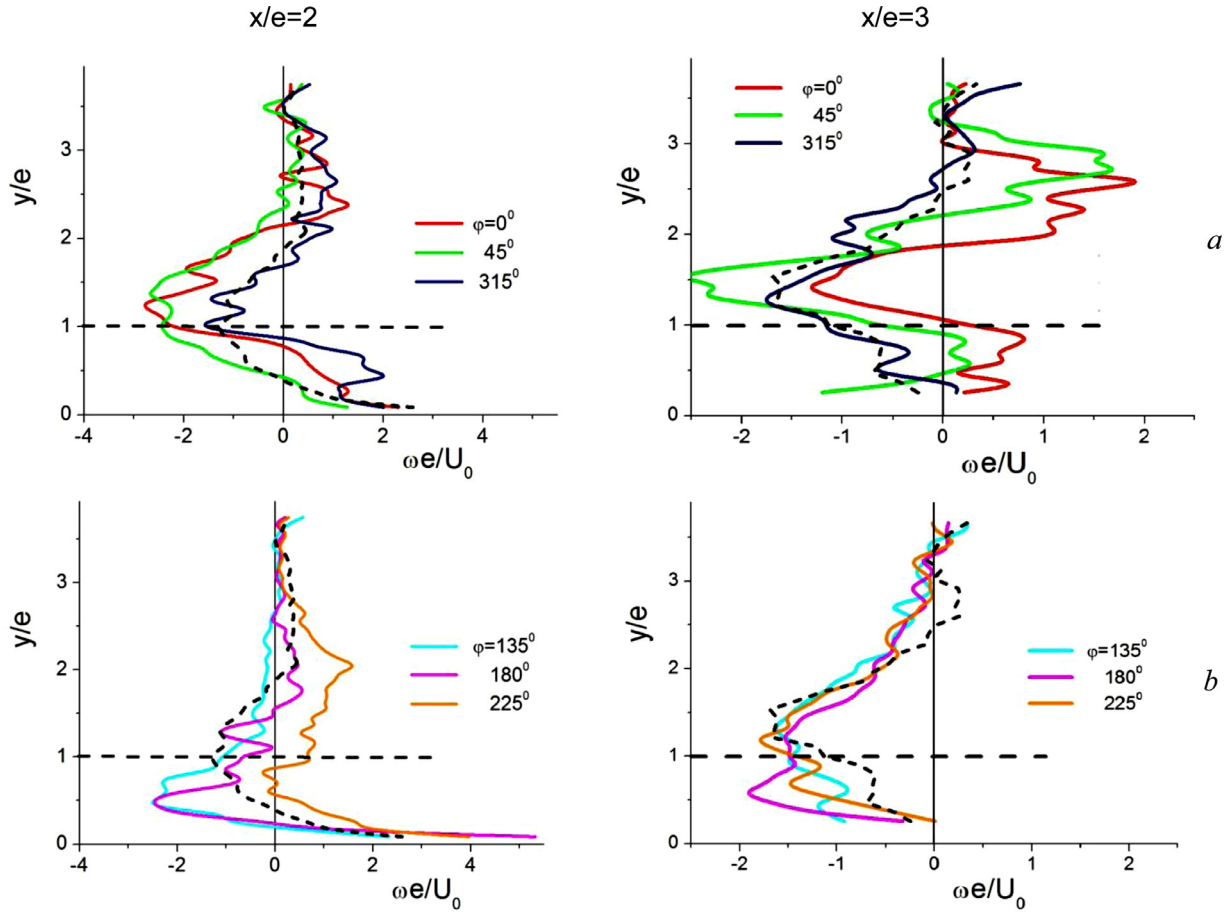

Fig. 9. Vorticity profiles at $x/e = 2$ (left column) and $x/e = 3$ (right column) in acceleration (a) and deceleration (b) phases.

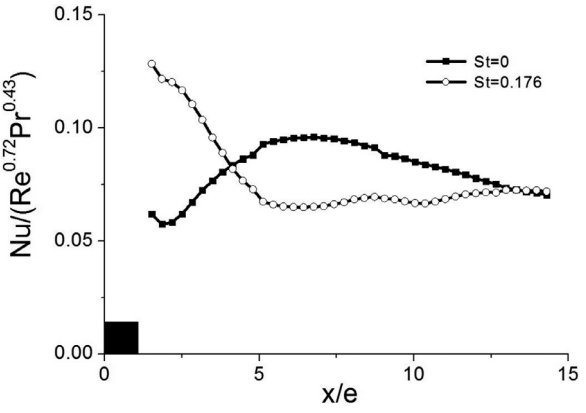

Fig. 10. Heat transfer coefficient in the separation region in steady and pulsating flows.

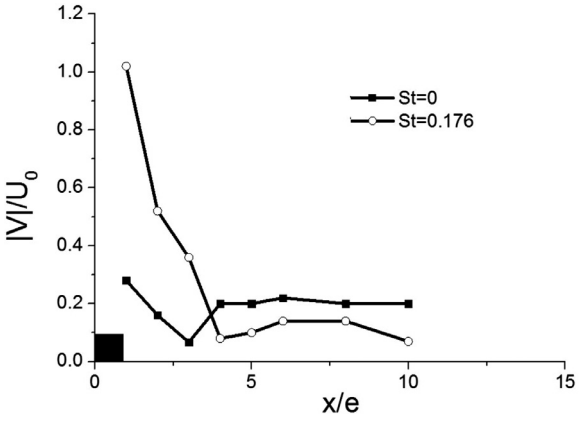

Fig. 11. Modulus of the transverse velocity.

Some scatter of points around the approximating line (1) is observed at the lowest transverse velocities almost immediately downstream of the separation region, $x/e>5$. However, the correlation is quite strong near the rib, where the flow pulsations (vortex generation) significantly promote the heat transfer. In general, stronger correlation is observed in pulsating flows (empty symbols in Fig. 12), in which the transverse velocity is more pronounced due to emerging vortices.

The obtained correlation contributes to deeper insight into the mechanisms of the influence of forced flow pulsations on convective heat transfer in the separation region behind an obstacle. The correlation implies that these complex flows exhibit rather strong interrelationship between time-averaged local heat transfer and time-averaged local maximum transverse velocity. In other words, when the space-time structure of the separation region is fundamentally rearranged under the influence of forced pulsations, there is a flow parameter which is in strong correlation with the local heat transfer. This parameter is the normalized transverse velocity near the wall, which represents the velocity of mass transfer in transverse direction. Large-scale vortical motion induced by flow pulsations enhances mass transfer in transverse direction and augments heat transfer. The obtained $Nu \sim |V|/U_0$ correlation cannot

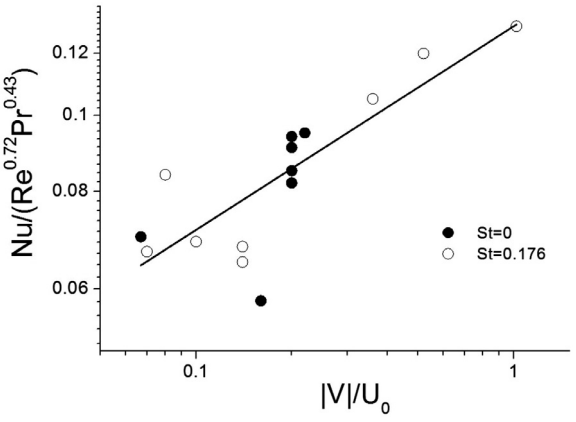

Fig. 12. Heat transfer coefficient vs transverse velocity: dots – experimental data; line – Eq. (1).

be considered universal, and we cannot recommend it for a large spectrum of problems yet. To do so, it must at least be tested for other types of flow. For example, strong transverse mass transfer may occur in separated steady flows in confined channels.

In our case, the applicability limits of the proposed correlation (1) are defined by the ranges of flow parameters considered in our study. Separated flows must be:

- subsonic $U<<a$ (a is the sound velocity);
- translatory (no reciprocating flows), i.e. the pulsation amplitude must be $\beta<1$;
- limited to the forcing frequencies St<0.2 in order to avoid fundamental rearrangement of vortical structure of separated flow.

Thus, the experimental data obtained in turbulent separated flows, including the pulsating flows, demonstrate that the location of maximum heat transfer coefficient almost coincides with the flow reattachment coordinate. Apart from the Reynolds number, the local heat transfer coefficient depends on the current normalized transverse velocity (its maximum value at each coordinate).

7. Conclusions

Experimental data on heat transfer and kinematic structure of the separated flow past a spanwise rib in a channel were obtained for steady and pulsating flow modes. In general, the forced flow pulsations were shown to enhance heat transfer compared to the steady flow case. The most pronounced augmentation of local heat transfer (up to three times compared to the steady flow at the same average flow rate) is observed in the near wake of the rib, i.e. at x=(1–5)e. The effect of forced flow pulsations on heat transfer distribution is generalized well using the non-dimensional frequency of forced flow pulsations (Strouhal number). At identical Strouhal numbers, the behavior of heat transfer coefficient along the separation region is similar. The Reynolds number to the power of 0.72 should be used to generalize the heat transfer distribution along the whole separation region length.

The study into kinematic flow structure based on SIV measurements of the dynamics of velocity vector fields allowed us to elaborate on the mechanisms of heat transfer enhancement. The heat transfer maximum is located close to the average reattachment point both in steady and pulsating flows. In the latter case, this point is shifted upstream towards the rib. In general, two different zones of kinematic structure of pulsating separated flows can be distinguished: core flow and vortical region. Close correlation between the local heat transfer coefficient and maximum transverse velocity at the respective coordinate was revealed suggesting that the transverse mass transfer initiated by forced pulsations plays an important role in heat transfer enhancement in the near wake of the rib. In qualitative and quantitative terms, the modulus of normalized transverse velocity agrees well with the behavior of heat transfer coefficient along the separation region in the considered flows: Nu~$(|V|/U_0)^{0.26}$.

Declaration of Competing Interest

The authors declare that they have no known competing financial interests or personal relationships that could have appeared to influence the work reported in this paper.

CRediT authorship contribution statement

I.A. Davletshin: Formal analysis, Writing - review & editing. **A.N. Mikheev:** Investigation. **N.I. Mikheev:** Conceptualization, Writing - review & editing. **R.R. Shakirov:** Investigation.

Acknowledgements

The study was financially supported by the Russian Science Foundation (grant no. 19–19–00355).

References

[1] P.K. Chang, in: Separation of Flow, Pergamon Press Ltd, Oxford, 1970, p. 796.
[2] M.A. Moon, M.J. Park, K.Y. Kim, Evaluation of heat transfer performances of various rib shapes, Int J Heat Mass Transf 71 (2014) 275–284.
[3] I. Elbadawy, Sabry Ali, H. Shedid Mohamed, A. Basheer, Heat transfer characteristics in wake region of a single finned obstacle, International Journal of Thermal Sciences 128 (2018) 149–159.
[4] R. Kumar, R. Chauhan, M. Sethi, A. Sharma, A. Kumar, Experimental investigation of effect of flow attack angle on thermohydraulic performance of air flow in a rectangular channel with discrete V-pattern baffle on the heated plate, Advances in Mechanical Engineering 8 (5) (2016) 1687814016641056.
[5] X.Y. Tang, G. Jiang, G. Cao, Parameters study and analysis of turbulent flow and heat transfer enhancement in narrow channel with discrete grooved structures, Chemical Engineering Research and Design 93 (2015) 232–250.
[6] S. Li, Z. Chorbani-Tari, G. Xie, B. Sundén, An experimental and numerical study of flow and heat transfer in ribbed channels with large rib pitch-to-height ratios, Journal of Enhanced Heat Transfer 20 (4) (2013) 305–319.
[7] E.A. Sewall, D.K. Tafti, A.B. Graham, Experimental validation of large eddy simulations of flow and heat transfer in a stationary ribbed duct, International Journal of Heat and Fluid Flow 27 (2) (2006) 243–258.
[8] G. Rau, M. Cakan, D. Moeller, T. Arts, The effect of periodic ribs on the local aerodynamic and heat transfer performance of a straight cooling channel, J Turbomach 120 (2) (1998) 368–375.
[9] K. Kant, A. Qayoum, Numerical investigations of fluid flow and heat transfer in a ribbed heated duct with variable aspect ratios, Recent Trends in Fluid Mechanics 3 (1) (2016) 23–37.
[10] M.A. Habib, S.A.M. Said, T. Ayinde, Characteristics of natural convection heat transfer in an array of discrete heat sources, Experimental Heat Transfer 27 (1) (2014) 91–111.
[11] L. Wang, B. Sundén, Experimental investigation of local heat transfer in a square duct with various-shaped ribs, Heat and Mass Transfer 43 (8) (2007) 759–766.
[12] F. Shin, Y. Wen-Jei, Z. Nengli, Local heat transfer in a rotating serpentine passage with rib-roughened surfaces, Int J Heat Mass Transf 37 (2) (1994) 217–228.
[13] S. Zheng, T. Ji, G. Xie, B. Sundén, On the improvement of the poor heat transfer lee-side regions of square cross-section ribbed channels, Numerical Heat Transfer, Part A: Applications 66 (9) (2014) 963–989.
[14] G. Xie, S. Zheng, W. Zhang, B. Sundén, A numerical study of flow structure and heat transfer in a square channel with ribs combined downstream half-size or same-size ribs, Appl Therm Eng 61 (2) (2013) 289–300.
[15] A.I. Leont'ev, V.I. Ivin, L.V. Grekhov, Semiempirical method of estimating the heat transfer level behind the boundary-layer separation point, Journal of Engineering Physics and Thermophysics 47 (4) (1984) 1134–1139.
[16] N.I. Mikheev, V.M. Molochnikov, I.A. Davletshin, O.A. Dushina, Simulation of pulsating channel flows, Russian Aeronautics 52 (1) (2009) 77–82.
[17] A.E. Goltsman, I.A. Davletshin, N.I. Mikheev, A.A. Paereliy, Shear stresses in turbulent pulsating channel flow, Thermophysics and Aeromechanics 22 (3) (2015) 319–328.
[18] P.K. Papadopoulos, A.P. Vouros, Pulsating turbulent pipe flow in the current dominated regime at high and very-high frequencies, International Journal of Heat and Fluid Flow 58 (2016) 54–67.
[19] A. Witte, W. Polifke, Dynamics of unsteady heat transfer in pulsating flow across a cylinder, Int J Heat Mass Transf 109 (2017) 1111–1131.

[20] H. Yuan, S. Tan, J. Wen, N. Zhuang, Heat transfer of pulsating laminar flow in pipes with wall thermal inertia, International Journal of Thermal Sciences 99 (2016) 152–160.
[21] P. Li, D. Guo, R. Liu, Mechanism analysis of heat transfer and flow structure of periodic pulsating nanofluids slot-jet impingement with different waveforms, Appl Therm Eng 152 (2019) 937–945.
[22] I.A. Davletshin, N.I. Mikheev, Flow structure and heat transfer during the separation of a pulsating flow, High Temperature 50 (3) (2012) 412–419.
[23] S. Amiri, R. Taher, L. Mongeau, Quantitative visualization of temperature field and measurement of local heat transfer coefficient over heat exchanger elements in sinusoidal oscillating flow, Experimental Thermal and Fluid Science 85 (2017) 22–36.
[24] I.A. Davletshin, Studies of separated flow downstream of the obstacle in a channel at resonant modes of pulsating flow, Russian Aeronautics 50 (3) (2007) 292–297.
[25] B. Cukurel, C. Selcan, M. Stratmann, Convective heat transfer investigation of acoustically excited flow over an isolated rib obstacle, Int J Heat Mass Transf 91 (2015) 848–860.
[26] F. Selimefendigil, H.F. Öztop, Forced convection and thermal predictions of pulsating nanofluid flow over a backward facing step with a corrugated bottom wall, Int J Heat Mass Transf 110 (2017) 231–247.
[27] A. Chamkha, F. Selimefendigil, Forced convection of pulsating nanofluid flow over a backward facing step with various particle shapes, Energies 11 (11) (2018) 3068.
[28] S. Šarić, S. Jakirlić, C. Tropea, A periodically perturbed backward-facing step flow by means of LES, DES and T-RANS: an example of flow separation control, J Fluids Eng 127 (5) (2005) 879–887.
[29] A. Das Gupta, P. Zhao, S. Roy, Plasma assisted turbulent flow separation control over a backward facing step, 54th AIAA Aerospace sciences Meeting, 2016 https://doi.org/10.2514/6.2016-0454.
[30] K.B. Chun, H.J. Sung, Control of turbulent separated flow over a backward-facing step by local forcing, Exp Fluids 21 (6) (1996) 417–426.
[31] S. Yoshioka, S. Obi, S. Masuda, Organized vortex motion in periodically perturbed turbulent separated flow over a backward-facing step, International Journal of Heat and Fluid Flow 22 (3) (2001) 301–307.
[32] G.H. Rhee, H.J. Sung, Enhancement of heat transfer in turbulent separated and reattaching flow by local forcing, Numerical Heat Transfer: Part A: Applications 37 (7) (2000) 733–753.
[33] R. Zhao, W. Li, W. Zhuge, Y. Zhang, Y. Yin, Y. Wu, Characterization of two-stage turbine system under steady and pulsating flow conditions, Energy 148 (2018) 407–423.
[34] I.A. Davletshin, N.I. Mikheev, A.A. Paereliy, I.M. Gazizov, Convective heat transfer in the channel entrance with a square leading edge under forced flow pulsations, Int J Heat Mass Transf 129 (2019) 74–85.
[35] A. Goltsman, I. Saushin, N. Mikheev, A. Paereliy, Generation of sinusoidal pulsating flows in the channels of experimental setups, Flow Measurement and Instrumentation 66 (2019) 60–66.
[36] M. Kiya, K. Sasaki, Structure of large-scale vortices and unsteady reverse flow in the reattaching zone of a turbulent separation bubble, J Fluid Mech 154 (1985) 463–491.
[37] L. Wang, M. Salewski, B. Sundén, Turbulent flow in a ribbed channel: flow structures in the vicinity of a rib, Experimental Thermal and Fluid Science 34 (2) (2010) 165–176.
[38] N.I. Mikheev, N.S. Dushin, A method for measuring the dynamics of velocity vector fields in a turbulent flow using smoke image visualization videos, Instruments and Experimental Techniques 59 (6) (2016) 882–889.
[39] V. Molochnikov, N. Mikheev, A. Mikheev, A. Paereliy, N. Dushin, O. Dushina, SIV measurements of flow structure in the near wake of a circular cylinder at Re=3900, Fluid Dyn Res 51 (2019) 055505.
[40] N.I. Mikheev, A.E. Goltsman, I.I. Saushin, O.A. Dushina, Estimation of turbulent energy dissipation in the boundary layer using Smoke Image Velocimetry, Exp Fluids (2017) 58–97.
[41] B.F. Armaly, F. Durst, J.C.F. Pereira, B. Schonung, Experimental and theoretical investigation of backward-facing step flow, J Fluid Mech 127 (1983) 473–496.
[42] F. Fouladi, P. Henshaw, D.S.-K. Ting, Steve Ray, Flat plate convection heat transfer enhancement via a square rib, Int J Heat Mass Transf 104 (2017) 1202–1216.